Automated analysis of single-molecule photobleaching data by statistical modeling of spot populations

Liesche, Clarissa; Grussmayer, Kristin S.; Ludwig, Michael; Woerz, Stefan; Rohr, Karl; Herten, Dirk-Peter; Beaudouin, Joel; Eils, Roland

DOI:
10.1016/j.bpj.2015.10.035

Biophysical Journal Volume 109 December 2015 2352–2362

Article

Automated Analysis of Single-Molecule Photobleaching Data by Statistical Modeling of Spot Populations

Clarissa Liesche,[1,2] Kristin S. Grußmayer,[3] Michael Ludwig,[3] Stefan Wörz,[1,2] Karl Rohr,[1,2] Dirk-Peter Herten,[3] Joël Beaudouin,[1,2] and Roland Eils[1,2,*]

[1]Division of Theoretical Bioinformatics (B080), German Cancer Research Center (DKFZ), Heidelberg, Germany; [2]Department for Bioinformatics and Functional Genomics, Institute for Pharmacy and Molecular Biotechnology (IPMB) and BioQuant, Heidelberg University, Heidelberg, Germany; and [3]CellNetworks Cluster and Institute for Physical Chemistry, BioQuant, Heidelberg University, Heidelberg, Germany

ABSTRACT The number of fluorophores within a molecule complex can be revealed by single-molecule photobleaching imaging. A widely applied strategy to analyze intensity traces over time is the quantification of photobleaching step counts. However, several factors can limit and bias the detection of photobleaching steps, including noise, high numbers of fluorophores, and the possibility that several photobleaching events occur almost simultaneously. In this study, we propose a new approach, to our knowledge, to determine the fluorophore number that correlates the intensity decay of a population of molecule complexes with the decay of the number of visible complexes. We validated our approach using single and fourfold Atto-labeled DNA strands. As an example we estimated the subunit stoichiometry of soluble CD95L using GFP fusion proteins. To assess the precision of our method we performed in silico experiments showing that the estimates are not biased for experimentally observed intensity fluctuations and that the relative precision remains constant with increasing number of fluorophores. In case of fractional fluorescent labeling, our simulations predicted that the fluorophore number estimate corresponds to the product of the true fluorophore number with the labeling fraction. Our method, denoted by spot number and intensity correlation (SONIC), is fully automated, robust to noise, and does not require the counting of photobleaching events.

INTRODUCTION

Several approaches have been developed to count fluorophores in molecule complexes. For example, fluorescence fluctuation spectroscopy can deliver the fluorophore number of moving complexes from an ensemble measurement (1,2). In contrast, one can also count fluorophores by imaging single molecules. Prominent techniques for this are localization microscopy such as photoactivated localization microscopy/stochastic optical reconstruction microscopy (3); counting by photon statistics (COPS), which relies on photon antibunching (4,5); or single-molecule photobleaching (SMPB) imaging (6,7). Those methods have different technical demands and different fluorophore requirements (5,8). In particular, SMPB imaging allows the use of both GFP-like fluorescent proteins and organic dyes and is technically easy to implement.

SMPB consists of photobleaching single fluorescent complexes while imaging them. Plotting the intensity over time of each complex generates a trace that appears as a staircase, with steps corresponding to the photobleaching of one or more individual fluorophores within the complex. The main methods used to infer the average fluorophore number per complex from photobleaching traces are the direct step-counting approach and the total-versus-single-step-intensity-ratio approach (9). The first approach consists in imaging until all fluorophores are photobleached and counting the number of photobleaching steps (6,7). In particular, fitting a binomial distribution to the step count histogram allows estimating the fluorophore number per complex, even when only a fraction of molecules in the population is labeled (10–12). In previous studies, this method was applied for small fluorophore numbers, for example, four (11), five (13), six (10), and seven (12) fluorophores. In the second approach, particularly relevant for higher numbers, the individual steps are not counted, but instead the fluorophore number is estimated by relating the initial intensity of single complexes and the intensity of single-step photobleaching (14,15). Photobleaching step identification was optimized with respect to instrumentation (16), noise minimization (17), and automatic step detection (12,13,18). Nevertheless, especially with the step-counting approach, it generally appears that the quality of the step identification has to be checked and the rejection of ambiguous traces has been reported (11–13).

While analyzing SMPB experiments with fluorescent proteins, we realized how challenging the step identification could be. Both the identification of all photobleaching steps for the counting analysis and the identification of single steps that could be used as a divider to estimate the stoichiometry from the initial intensity appeared difficult and

Submitted June 5, 2015, and accepted for publication October 26, 2015.

*Correspondence: r.eils@dkfz.de

Joël Beaudouin and Roland Eils contributed equally to this work.

Editor: Keir Neuman

0006-3495/15/12/2352/11

http://dx.doi.org/10.1016/j.bpj.2015.10.035

subjective. The main reason for this limitation is the presence of noise. Therefore, we set out to explore a method to estimate the fluorophore number from SMPB intensity-time traces independent of step identification. Our proposed method consists of relating the fluorescence intensity decay of a population of complexes to the decay of the number of visible complexes. All the fluorophores within the complex, visible as a diffraction-limited spot, have to be photobleached for the spot to disappear. Therefore, if a complex contains more than one fluorophore, the spot number decay appears slower than the fluorescence intensity decay. We developed a statistical model to quantitatively interpret this delay to estimate the average fluorophore number per complex.

As a proof of concept, our method allowed the correct estimation of single- and fourfold-labeled DNA probes with three different fluorescent dyes, Atto542, Atto565, and Atto647N. We could also determine with GFP fusions that the soluble form of human CD95 ligand, which binds to the death receptor CD95 but has a weak capacity to induce apoptosis, remains trimeric in the picomolar range. Using computer simulations, we found that our method is robust to noise and therefore particularly relevant for SMPB performed with fluorescent proteins. It tolerates limited fluorophore blinking, and because the method is based on statistical analysis of multiple fluorescent traces, we observed that the accuracy improved with increasing spot numbers per analyzed image region. Moreover, simulations predicted that our method can be used to estimate a high number of fluorophores per complex. Interestingly, when fluorescence labeling of the analyte is incomplete, the fluorophore number estimate corresponds to the product of the labeling fraction with the number of fluorophores if labeling was complete. In this context, using a priori knowledge of one of the two parameters, the fluorophore number or labeling fraction, allows for the direct estimation of the other. Our method is an attractive approach for the analysis of SMPB data as it does not rely on individual photobleaching step detection, the most laborious and subjective part of previous approaches. Importantly, the analysis of intensity traces is fully automated and permits the use of the total set of traces without having to reject the ambiguous ones.

MATERIALS AND METHODS

Preparation of DNA probes

Oligonucleotides were custom synthesized and purified using high-performance liquid chromatography (HPLC) by Sigma-Aldrich (Taufkirchen, Germany) or by biomers.net (Ulm, Germany). NHS-ester and azide-modified Atto647N, Atto542, and Atto565 were bought from ATTO-Tec (Siegen, Germany). The tetra probes consist of a biotinylated DNA strand with 94 bases of four 23-base repeats (tetra′) and the complementary strand (tetra). Tetra contains four 2′-O-Propargyl uridine (pU) bases that are coupled to the respective azide-modified dye and purified using HPLC by biomers.net. All sequences are given 5′-3′. Tetra′: C6 Amine-AAC GAG GAG GAC CCC TAT CCC AAA ACG AGG AGG ACC CCT ATC CCA AAA CGA GGA GGA CCC CTA TCC CAA AAC GAG GAG GAC CCC TAT CCC AA- Biotin. Tetra: (pU)TG GGA TAG GGG TCC TCC TCG TT(pU) TGG GAT AGG GGT CCT CCT CGT T(pU)T GGG ATA GGG GTC CTC CTC GTT UTG GGA TAG GGG TCC TCC TCG TT. The mono probes consist of a biotinylated DNA strand with 22 bases that is modified with the NHS-ester of the respective dye via a C6 amine linker and the complementary strand (mono′). Mono′: AAA AAC GCA AAG CAA GCG CGG G. Mono: Biotin-CCC GCG CTT GCT TTG CGT TTT T-C6 Amine. Contrary to the tetra probes, mono probes were labeled and purified by ourselves as previously reported (4). Tetra probes and mono probes were formed by adding the respective two complementary DNA strands in a 1:1 ratio (1 μM) in 1× phosphate buffer solution (PBS) followed by hybridization through heating to 90°C for 4 min and subsequent cooling to 25°C (1°C in 30 s) in a thermocycler (PTC-100, MJ Research, Waltham, MA).

Absorption measurements

Ensemble UV-Vis absorption measurements with a Cary 500 Scan UV-Vis spectrometer (Varian, Darmstadt, Germany) were used to calculate the degree of labeling (DOL) of the DNA samples in PBS pH 7.4. Absorption measurements were baseline corrected against pure solvent. The DOL was computed via Lambert-Beers' law as the relative concentration of fluorophores and DNA in the solution using the known molar extinction coefficients ε_max and ε_DNA of the dye and the DNA at the absorption maximum and at 260 nm, respectively, and the correction factors (CF) provided by the manufacturer. The DOL = (A_max/ε_max)/(A_DNA/ε_DNA) = (A_max*ε_DNA)/((A_260-CF*A_max)*ε_max), with A_max being the absorbance at the absorption maximum of the dye, and A_260 the absorbance at 260 nm.

Single-molecule surface preparation

All experiments were conducted in Lab-Tek chambered coverslides as in an earlier study (4) In brief, the slides were cleaned twice with hydrofluoric acid (0.1 M) for 5 min, followed by three washes with 1× PBS. To functionalize the glass surface, BSA and BSA-Biotin (20:1 ratio, 5 mg/mL total) were incubated for 30 min at room temperature followed by three washes with 1× PBS and subsequently treated with streptavidin (0.1 mg/mL) for 20 min followed by three washes with 1× PBS. Experiments with Atto647N were performed with an enzymatic oxygen scavenging system and reducing and oxidizing agents (ROXS) to stabilize dye fluorescence and reduce blinking (19,20). We used a 5× PBS buffer containing glucose (300 mM), glycerol (12.5% v/v), and 2 mM Trolox (~12% converted to Trolox quinone by exposure to UV light) that was saturated with argon. Shortly before measurements were taken, we added Tris (2-carboxyethyl)phosphine (TCEP, 1mM), glucose oxidase (2 units/mL), and catalase (250 units/mL). We sealed the Lab-Tek chamber with Parafilm (BRAND, Wertheim, Germany) to avoid reintroduction of atmospheric oxygen. For immobilization of proteins, purified protein was diluted to a concentration of ~1 ng/ml in 1×PBS and added to a clean Lab-Tek chamber. The solution was incubated for 20 min and was then replaced by PBS.

DNA plasmids and protein expression

mGFP (21) and mCherry alone and fused to isoleucine zipper soluble CD95L (IZsCD95L) (22), to sCD95L and to IZ were cloned with a secretion signal and a flag-tag in pIRES-puro2 (CLONTECH, see Supporting Material for the details). 293T cells were cultured at 37°C and 5% CO2 in a humidified atmosphere in DMEM without phenol red (GIBCO, Thermo Fisher Scientific, Waltham, MA), supplemented with 10% FCS (BIOCHROM GmbH, Berlin, Germany), 2 mM L-Glutamin (GIBCO), and 100 units/ml penicillin with 100 μg/ml streptomycin (GIBCO). Cells

were transfected with the different DNA constructs using jetPRIME (VWR International GmbH, Erlangen, Germany) and medium was replaced 1 day later. The cell supernatant was collected 2 days after being washed, centrifuged, and filtered through a 0.22 μm PVDF-filter (MERCK Millipore, Billerica, MA). Proteins were purified at 4°C using ANTI-FLAG M2 Affinity Gel and 3× FLAG Peptide (Sigma-Aldrich) diluted in 1× PBS. Flag-Peptide was removed by size exclusion through centrifugation using Amicon Ultra-0.5 mL Centrifugal Filters (MERCK Millipore). Proteins were kept at 4°C or on ice and were protected from light until imaging.

Single-molecule imaging

Microscopy imaging was performed at room temperature on a custom total internal reflection fluorescence (TIRF) microscope equipped with an iXon plus emCCD camera (Andor, Dublin, Ireland) and a filter set (excitation dichroic: z488/633 or z532/633, triple-notch 488/532/631-640 nm, detection dichroic: 640 DCXR) allowing for dual-color excitation and detection (23). All filters were from AHF Analysentechnik (Tübingen, Germany). The incoming laser light was s-polarized, so perpendicular to the plane of incidence defined by the incoming and reflected laser beam. GFP was excited at 488 nm (PC13781, 40 mW, Spectra-Physics, Darmstadt, Germany), Atto542 and Atto565 at 532 nm (TECGL-30, World Star Tech, Toronto, Canada), and Atto647N at 640 nm (iBEAM-SMART-640-S, TOPTICA, Munich, Germany). Emission of GFP, Atto542, and Atto565 was passed through the short-wavelength channels BP 512/25, BP 585/65, and BP 593/46, respectively, and emission of Atto647N was passed through the long-wavelength channel BP 685/70. For GFP, Atto542, Atto565, and Atto647N, we acquired 400, 1000, 1000, and 2000 images for each time series, respectively, and at ~75, 150, 150, and 300 W/cm^2 power, respectively. For GFP, Atto542, and Atto565, images were acquired at 10 Hz using a gain of 200, and for Atto647N we used 1 Hz and set the gain to 50.

Image processing

In our experiments, the illumination of the region of view was stronger in the center (Fig. S1 *A* in the Supporting Material). This feature is inherent to TIRF illumination and represents only a current technical limitation that will certainly be improved in the future. As our image analysis approach requires that all molecules have an equal probability to be bleached, we subdivided images into smaller regions, where the illumination strength, estimated from the spot intensity from the first image of the time series, was similar (Fig. S1 *B*).

Spot feature extraction

Time series images were analyzed by an extension of the model-based segmentation approach (24) (see Supporting Material). The spot intensity was obtained by fitting a two-dimensional Gaussian profile. The basal line of the fit was defined as the background a_0. The spot intensity was obtained by subtracting a_0 from the parameter a_1 describing the amplitude of the fitted function. All intensity traces showing complete photobleaching were considered.

Spot quantification and computer simulations

We used MATLAB (The MathWorks GmbH, Ismaning, Germany) for the analysis of SMPB intensity profiles and to perform in silico experiments. To determine the spot number over time, the time point of spot disappearance was automatically extracted by determining when the Gaussian intensity fitting procedure of identified spots failed in consecutive images. We found that this strategy worked well for our image data (Fig. S2, A–C). The measured spot number decay $N(t)$ was normalized to 1 at time point 0. Intensity normalization was performed by dividing with the average intensity of the first four time points. For the fit, intensity values until the time point of spot disappearance were included. To fit the average fluorophore number per complex in our data, we applied least square minimization with the trust-region method. To simulate random numbers following an exponential distribution, we calculated the absolute value of the natural logarithm of a random number uniformly distributed between 0 and 1. Those numbers were multiplied by a factor to stretch the distribution on the corresponding timescale. To quantify intensity fluctuations, Gaussian function fits were applied (OriginLab, Northampton, MA).

RESULTS AND DISCUSSION

Theory

Our aim was to identify the fluorophore number in molecule complexes from SMPB data without counting individual photobleaching steps. We used two features from the data that can be easily determined: the total fluorescence intensity $I(t)$ of all the spots within one field, which we normalized to 1 at time point 0, and the number of spots over time $N(t)$. These two features are intuitively related: whereas $I(t)$ depends only on the fluorophore properties, $N(t)$ depends on both the fluorophore properties and the fluorophore number per spot (Fig. 1 *A*). The more labels a spot contains, the longer the spot stays visible because all the labels within the spot need to be bleached for it to disappear. If $p(t)$ is the probability for a molecule to be fluorescent at time t, then the probability for a complex containing n fluorophores to have disappeared at that time is $(1 - p(t))^n$. Therefore, the probability for a spot to be fluorescent at time t is $1 - (1 - p(t))^n$. The measured fluorescence intensity $I(t)$ represents an approximation of $p(t)$. Hence, the spot number $N(t)$, normalized to 1 at time 0, can be derived from the intensity $I(t)$ as in the following:

$$N(t) = 1 - (1 - I(t))^n. \quad (1)$$

Although the total intensity of the spots decays immediately at the start of imaging, the spot number decay shows a plateau before decay for spots containing more than one fluorophore. The more labels a spot contains, the longer this plateau lasts (Fig. 1 *B*).

From the measured intensity of a spot population $I_{data}(t)$, one can determine the expected spot number over time $N_{exp}(k,t)$ using Eq. 1 for any fluorophore number k. We hypothesized that we could estimate the true fluorophore number n by fitting $N_{exp}(k,t)$ to the measured spot number decay $N_{data}(n,t)$. For this, we estimated the parameter k that minimized the following equation:

$$\sum_{t=0}^{t_x} \left(N_{data}(n,t) - N_{exp}(k,t)\right)^2, \quad (2)$$

where k is a real number, t_x is the time when all spots are bleached, and $N_{exp}(k,t)$ is the following:

$$N_{exp}(k,t) = 1 - (1 - I_{data}(t))^k. \quad (3)$$

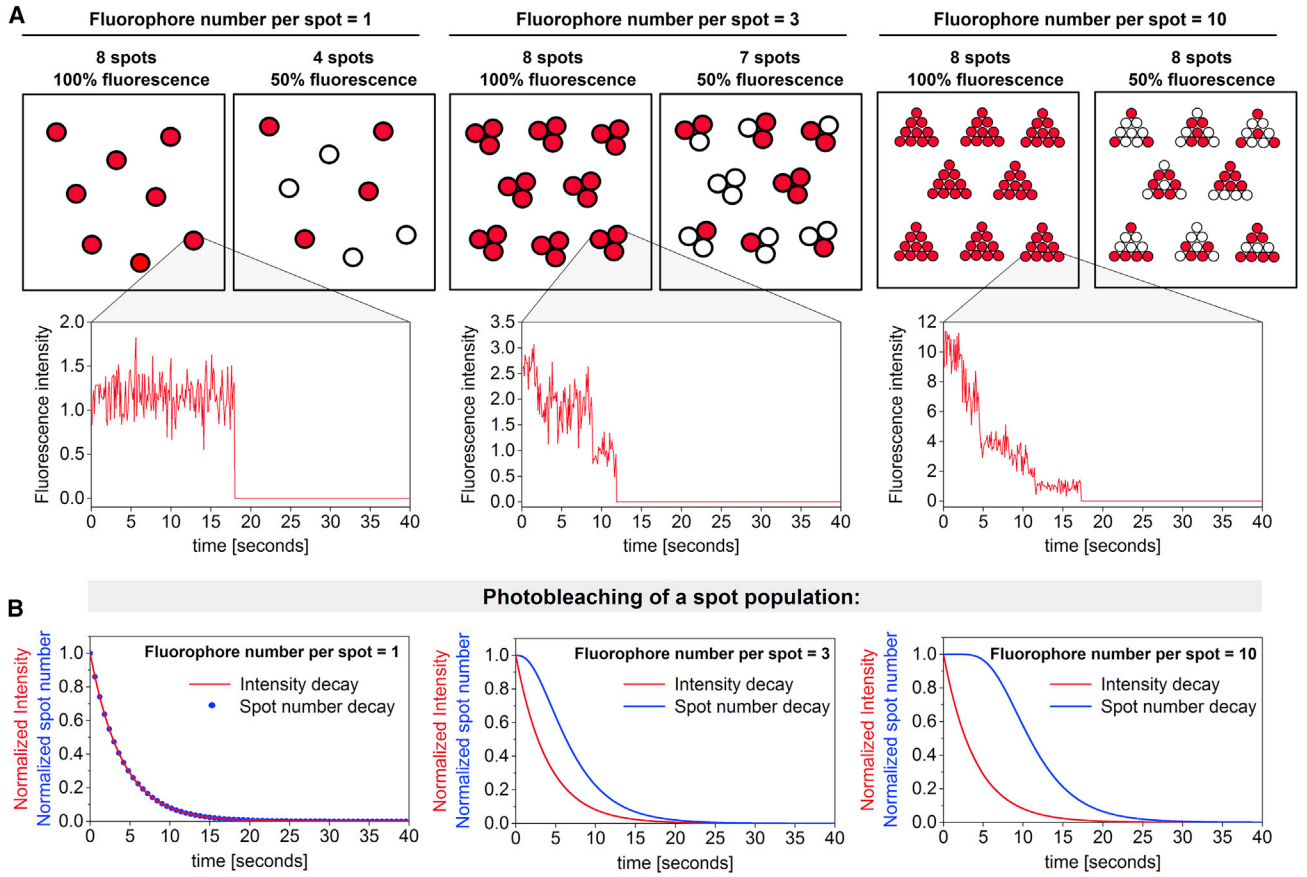

FIGURE 1 (*A*) Scheme of 8 spots containing 1 (monomer), 3 (trimer), or 10 (decamer) fluorophores per spot. When half of the fluorophores in a spot population are photobleached (50% fluorescence), half of the monomers, but statistically only 12.5% trimers are fully photobleached. For decamers, 0.1% of the spots would be fully photobleached in this case. Graphs are simulations of SMPB intensity-time traces of a single spot with 1, 3, or 10 fluorophores (see section simulations below). (*B*) Theoretical spot number and intensity decay for different fluorophore numbers per spot. The fluorescence intensity from a population of molecules was assumed to decay exponentially over time (*red line*). Because of the normalization to 1 at time 0, the intensity decay is the same in all three cases shown here. Although the spot number decay equals the intensity decay for a fluorophore number $n = 1$ (*blue circles*), the spot number decay displays a clear lag phase for complexes with fluorophore numbers larger than 1 (*blue line*).

In SMPB experiments that are analyzed by counting photobleaching steps, the obtained histogram is often interpreted assuming a second parameter, the fluorescent fraction of labels (10–12). This can be realized with our approach using the same formalism as above because a fluorescent fraction α at time 0 is equivalent to a delay in the start of the measurement of a sample having 100% fluorescent labels at time 0. The intensity at time 0 with a fluorescent fraction α is equal to α*$I(0)$. This means that Eq. 1 remains valid with a time shift Δt.

$$\begin{aligned} N_{fraction}(t) &= 1-(1-I(t+\Delta t))^n \\ &= 1-(1-I(t)\times\alpha)^n, \text{with} \\ I &= [0,1] \\ I(0) &= 1 \\ \alpha &= [0,1]. \end{aligned}$$

By normalizing this spot number decay to 1 at time point 0, one can derive the expected number of spots over time for a fluorophore number k using Eq. 4 in the following:

$$N_{exp}(k,\alpha,t) = \frac{1-(1-I_{data}(t)\times\alpha)^k}{1-(1-\alpha)^k} \qquad (4)$$

Compared with the photobleaching step-counting approach, the method presented here relates the kinetics of spot disappearance with the intensity decay, we thus termed our method spot number and intensity correlation (SONIC).

Counting fluorophores on DNA standards

To validate our method, we used mono- and tetra-DNA probes containing one (Fig. 2 *A*) and four (Fig. 2 *B*) fluorophore labels with Atto542, Atto565, or Atto647N. First, we estimated their degree of labeling using absorption spectrometry (Table 1). The calculated labeling efficiency was close to four for tetra-Atto565 and tetra-Atto647N, and to

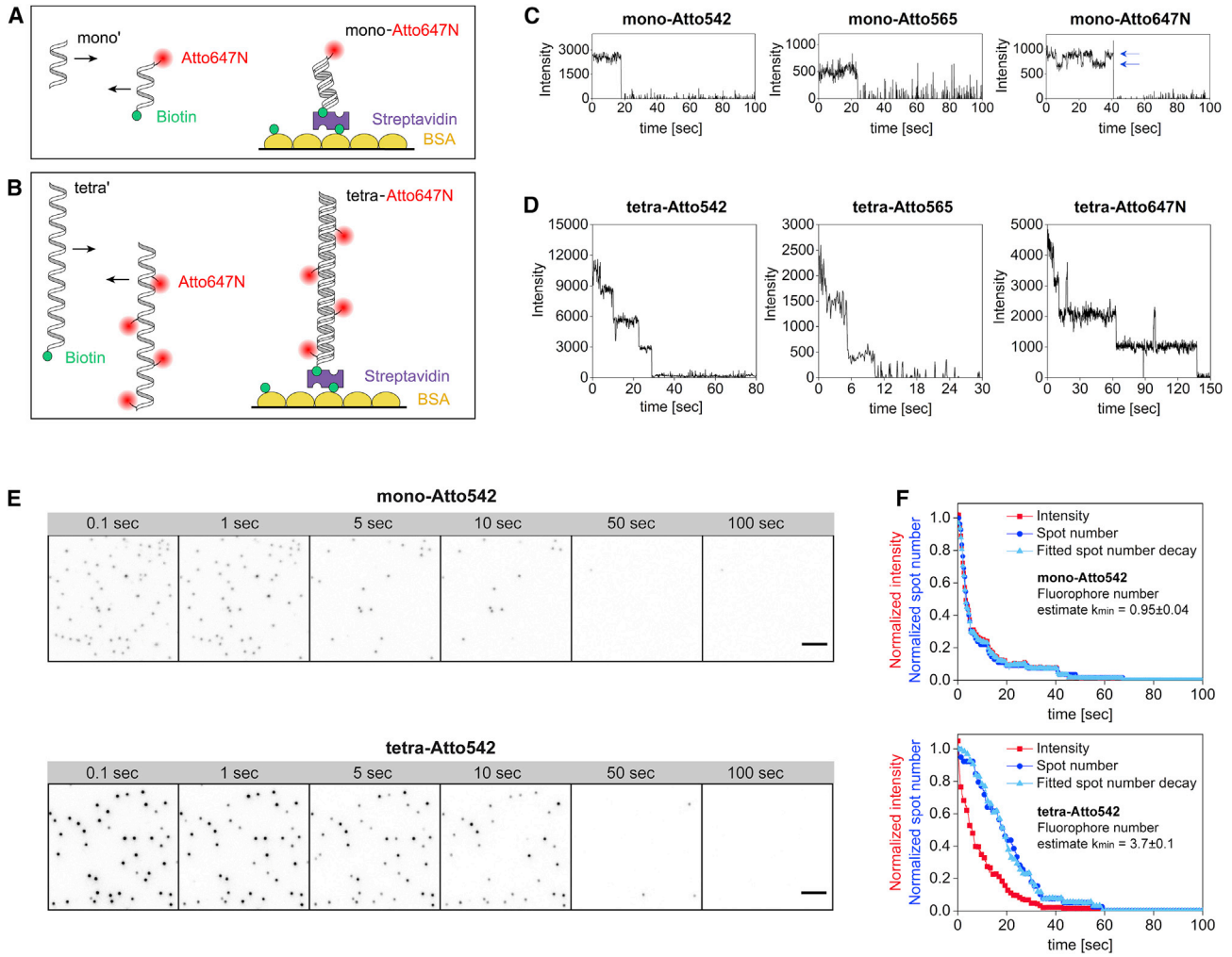

FIGURE 2 (*A*) DNA probes with single dye that carried a biotin and a fluorescent dye on the same DNA strand. (*B*) DNA probes with four dyes that contained a biotinylated strand and a complementary one carrying the dyes. (*C*) Example SMPB intensity-time traces of DNA mono probes and (*D*) tetra probes labeled with Atto542, Atto565, and Atto647N. In addition to the expected photobleaching steps, transient shifts of mean intensity could be observed (see *arrows* for mono-Atto647N). (*E*) Time series images of tetra-Atto542 probes and mono-Atto542 probes. Scale bar = 1 μm. (*F*) Fluorescence intensity and spot number quantification of time series images from (*E*). Although the intensity decay occurs on the same timescale for both DNA probes, the spot number decay was slower than the intensity decay for the tetra-Atto542 probe, and both decays overlapped for the mono-Atto542 probe. Eqs. 2 and 3 were used for spot number fits (*light blue triangles*). To see this figure in color, go online.

one for the mono-DNA probes. The only exception was for the tetra-Atto542, with 5.4 ± 1.1. As the negative charges of the DNA and the dye exclude a nonspecific interaction, and as there are only four binding sites on the DNA, an overlap of the peaks of labeled DNA and free dye is likely the source for this high value. DNA probe imaging and spot quantification are described in the experimental section. Two different spot densities were measured, with an average

TABLE 1 Fluorophore number estimates of Atto-labeled DNA probes

Method/DNA Probe	Mono-Atto542	Mono-Atto565	Mono-Atto647N	Tetra-Atto542	Tetra-Atto565	Tetra-Atto647N
DOL[a]	0.9 ± 0.2	0.9 ± 0.2	1.1 ± 0.2	5.4 ± 1.1	3.9 ± 0.8	3.7 ± 0.7
Intensity ratio, high snr	1.11 ± 0.06 ($n = 5$)	1.20 ± 0.07 ($n = 5$)	1.04 ± 0.05 ($n = 3$)	3.76 ± 0.20 ($n = 5$)	4.80 ± 0.25 ($n = 5$)	4.00 ± 0.08 ($n = 6$)
SONIC, high snr	1.07 ± 0.09 ($n = 5$)	1.23 ± 0.11 ($n = 5$)	1.14 ± 0.15 ($n = 3$)	3.92 ± 0.42 ($n = 5$)	4.52 ± 0.64 ($n = 5$)	4.31 ± 0.59 ($n = 6$)
SONIC, low snr	1.01 ± 0.11 ($n = 14$)	1.25 ± 0.22 ($n = 15$)	1.10 ± 0.23 ($n = 8$)	4.06 ± 0.96 ($n = 21$)	4.12 ± 1.12 ($n = 14$)	

n, number of image regions; snr, spot number per image region.
[a]Ensemble degree of labeling with an estimated error of 20%.

number per image region of 41 ± 19 spots and 10 ± 2 spots and with total spot numbers ranging between 108 and 333 for the different DNA probes (Fig. S3). As expected, we observed one photobleaching step with mono probes and up to four photobleaching steps with tetra probes (Fig. 2, *C* and *D*). To note, transient changes of the mean intensity could be observed for Atto647N probes (see *arrows* in Fig. 2 *C*), likely representing two different emitting states/spectral forms of the fluorophore (19,20). First, as we could reasonably identify photobleaching steps with the different Atto-dyes, we measured the mean of the initial intensities and the mean of intensities of step that visually corresponded to single photobleaching events. This was performed for the experiments with the high number of spots per image region. From their ratio, we then estimated the fluorophore number of the different probes (Table 1). The obtained average fluorophore number per spot for Atto542 and Atto647N probes were in good agreement with the expected ones, but they were higher than expected for the Atto565 probe.

We then compared those results with the estimation generated by the SONIC approach. For this, we measured the spot number over time as described in the experimental section and estimated the fluorophore number by fitting this measured spot number decay to the one calculated from the intensity decay (Eqs. 2 and 3). Fig. 2 *E* shows image regions of mono-Atto542 and of tetra-Atto542 probes. Despite similar intensity decays, the spot number decay of tetra-Atto542 was clearly delayed compared with the one of mono-Atto542 (Fig. 2 *F*). For those example images, the estimated average fluorophore number was 0.95 ± 0.04 (fit ± 95% confidence interval) for the mono-Atto542 probe and 3.7 ± 0.1 for the tetra-Atto542 probe. We performed this analysis for the different acquired fields, the different probes, and the two different spot densities. The obtained values were in good agreement with the expected fluorophore numbers and also with the estimated ones from the intensity ratio approach (Table 1). In particular, the ranking of the fluorophore number with the different dyes was the same, with slightly higher fluorophore number estimates for mono- and tetra-Atto565 probes. Therefore, we concluded that using the SONIC approach, the number of fluorophores could be easily and automatically determined without bias.

Identifying the degree of multimerization of GFP-tagged proteins

We next aimed at testing our method using GFP, which generates less photons than the organic dyes used above. We analyzed the oligomerization of the soluble form of the TNF family member CD95L (sCD95L), which, contrary to its membrane counterpart, is a poor inducer of apoptosis. Soluble CD95L was reported to form trimeric assemblies, as determined by biochemical cross-linking with Western blotting and gel filtration (25,26). Here, we asked if sCD95L remains trimeric when diluted to picomolar concentration, or if it dissociates into monomers as proposed for the related ligand TNF-α (27,28). For this, we genetically fused the ligand to flag-tagged GFP (GFP-sCD95L) and compared it to three different GFP-fusions: a trimeric reference protein termed isoleucine zipper (29) (GFP-IZ), the strong apoptosis inducer IZsCD95L (25) (GFP-IZsCD95L), and monomeric GFP alone. Recombinant proteins were expressed and secreted by HEK 293T cells and purified by affinity chromatography. The integrity of the protein was checked by Western blotting. Although GFP, GFP-IZ, and GFP-sCD95L looked intact, GFP-IZsCD95L showed proteolytic cleavage of 8% of the full-length protein (Fig. S4). Fluorescence correlation spectroscopy (FCS), fluorescence cross-correlation spectroscopy, and biochemical cross-linking with Western blotting confirmed the multimeric state of GFP-tagged and mCherry-tagged IZ, sCD95L, and IZsCD95L in the nanomolar range (Figs. S5 and S6).

We imaged immobilized GFP-tagged proteins on glass and measured a total number of 88, 392, 237, and 192 spots and a mean spot number of 10 ± 3, 10 ± 3, 11 ± 3, and 10 ± 3 per region for GFP, GFP-IZ, GFP-sCD95L, and GFP-IZsCD95L, respectively, analogous to our measurements with DNA probes at sparse density. We observed individual photobleaching traces of sCD95L, IZ, and IZsCD95L fused to GFP with up to three bleaching steps whereas GFP molecules showed only single-step photobleaching (Fig. 3 *A*).

By applying the SONIC approach, we estimated a mean fluorophore number of 1.15 ± 0.54, 3.07 ± 0.70, and 2.97 ± 1.19 for GFP, GFP-IZ, and GFP-sCD95L spots, respectively (± SD of different regions, see Fig. 3, *B* and *C*). For GFP-IZsCD95L, the estimated fluorophore number was 2.72 ± 0.80 when assuming a labeling fraction of 100% ($p = 1$) and was 2.94 ± 0.89 when using Eq. 4 assuming $\alpha = 0.92$. We concluded from these results, that sCD95L is trimeric even when diluted to the picomolar range. Therefore, sCD95L trimers appear more stable than the human TNF-α and glucocorticoid-induced TNFR-related ligand (27,28,30–32). Moreover, although IZ-sCD95L is a more potent inducer of apoptosis than sCD95L, our observation indicates that the oligomerization degree alone is not sufficient to explain the activity difference, similar to what has been reported previously (25,26). We designed our experiments so that we could compare the proteins of interest with monomeric and trimeric calibrations. Notably, we observed that the fitted fluorophore numbers were actually matching the expected ones, indicating a close to complete maturation of the GFP. This contrasts with previous SMPB studies that interpret the distribution of photobleaching step counts in terms of a limited maturation of the fluorescent protein or labeling degree, with fractions ranging between 0.5 and 0.8 (11,13,33).

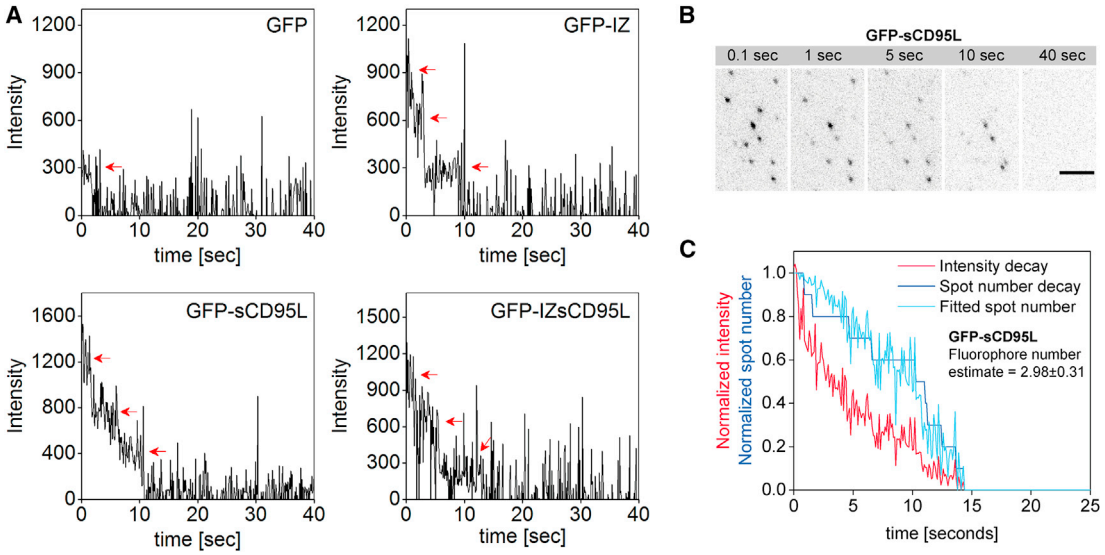

FIGURE 3 (*A*) Examples of intensity traces over time showing one photobleaching step for GFP and three photobleaching steps (*arrows*) for GFP-IZ, GFP-sCD95L, and GFP-IZsCD95L. (*B*) Snapshots of time series images of GFP-sCD95L. Scale bar = 1 μm. (*C*) Fluorescence intensity and spot number quantification of time series images from (*B*). The fit of the spot number from the intensity data was made using Eqs. 2 and 3 and predicted a fluorophore number of 2.98 $\pm$ 0.31 ($\pm$ 95% confidence interval).

Our observation would rather be consistent with the typical assumption of complete maturation made in the photon counting approach using FCS (2). A possible explanation is that the expression system used here may have led to higher GFP maturation than protein expression in bacteria or in *Xenopus* oocytes, often used for SMPB. Further work with samples that are compatible with different quantitative approaches like SMPB and FCS will certainly scrutinize this aspect.

Accuracy and precision of the SONIC approach

To investigate the potential bias and the sensitivity of our analysis approach, we applied it to simulated data. To mimic intensity traces over time, we generated random, exponentially distributed values that define the time point of fluorophore photobleaching. The mean intensity of each fluorophore was assumed to be 1 before and 0 after photobleaching. To estimate the relevant intensity fluctuations for the simulations, we measured the intensity distribution of the different dyes used in this study. Intensity fluctuations were reasonably described by a Gaussian distribution with a standard deviation normalized to the mean ranging from 0.1 for Atto-dyes to 0.4 for GFP (Fig. S7). Therefore, in simulations, intensity fluctuations were introduced by adding random values from Gaussian distributions centered at 0.

In the following, we investigated the potential bias and the sensitivity of our approach depending on the fluorophore number, noise, number of spots per image, and image number. Moreover, several biophysical effects such as the blinking, homo-FRET, effect of laser polarization, and constrained rotational diffusion or optical limitations such as the distance of the fluorophore from the glass can affect the experiment. Although testing all the effects would go beyond the scope of the study, we investigated the limits of the approach with blinking fluorophores. Furthermore, we explored the bias introduced by low labeling efficiencies.

First, to explore the range of fluorophore numbers that can be analyzed with our method, we simulated 20 times the photobleaching of 10 spots. Fluorophore numbers were varied from $n = 1$ to 30 with intensity fluctuations of $\sigma = 0.4$. Strikingly, the mean value of the estimated fluorophore number corresponded to the expected one over the whole range (Fig. 4 *A*). Thus, although future work will be needed to test the experimental validity, the SONIC approach may be used to estimate large fluorophore numbers.

Next, we tested the accuracy of the method for increasing intensity fluctuations σ by estimating the fluorophore numbers $n = 1$, 3, and 10. Whereas for $n = 1$ the fluorophore number was correctly estimated and independent of intensity fluctuations, correct estimates were obtained for $n = 3$ and $n = 10$ for σ lower than 1, which we observed experimentally. The fluorophore numbers were underestimated only if σ became larger than 1 (Fig. 4 *B*).

Besides, we also observed that the mean intensity of the different traces within a region fluctuated (Fig. S8). Apart from inhomogeneous illumination of the field, other sources may contribute to this effect such as varying distance of the dyes from the glass or the constrained rotational mobility of the dye. As explained in Fig. S8, we estimated the spread of this variation, leading to a standard deviation of $\sigma_{mean} =$ 0.15 times the intensity mean. By applying the SONIC analysis on simulations of 10 replicates with each 14 spots,

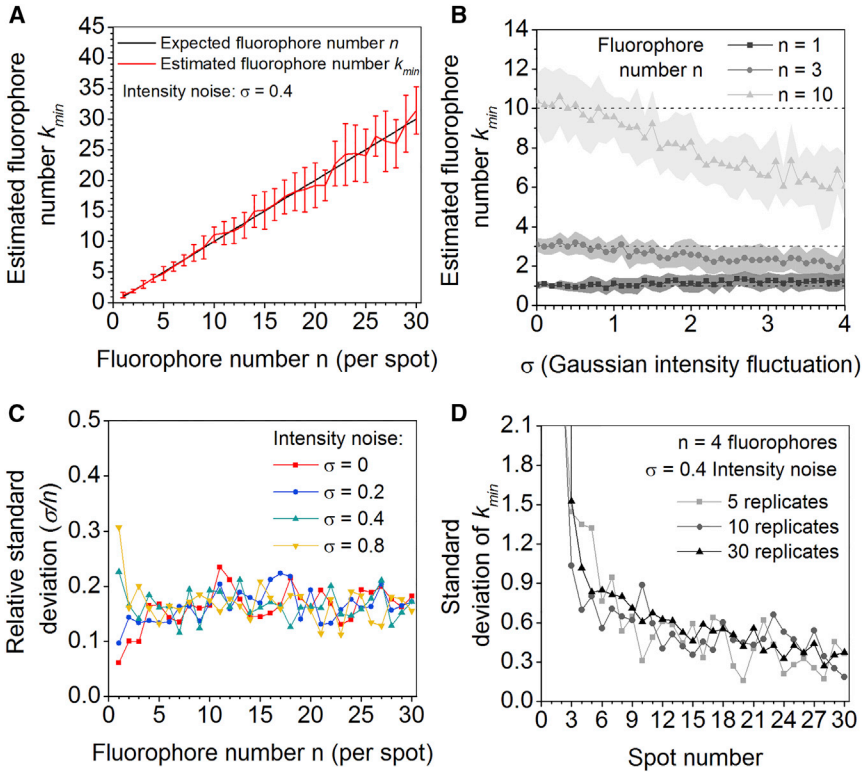

FIGURE 4 Effect of increasing intensity fluctuations, fluorophore numbers, and spot numbers on the bias and sensitivity. (*A–C*) Simulation of the photobleaching of 10 spots in 20 replicates and fluorophore number estimates (k_{min}) were obtained using the SONIC approach. (*A*) The red line indicates mean ± SD of k_{min} values overlapped with the expected number (*black*), indicating the absence of bias. (*B*) Mean ± SD (*shaded area*) of k_{min} for $n = 1$, 3, or 10 fluorophores, and for increasing Gaussian intensity fluctuations σ. Note that k_{min} for $n = 3$ and 10 starts deviating from expected values (*dashed line*) for σ above 1.0. (*C*) The relative standard deviation (SD/*n*) remains constant when plotted against the simulated fluorophore number per spot and is independent of tested intensity fluctuations $\sigma = 0$, 0.2, 0.4, or 0.8. (*D*) Spots with $n = 4$ fluorophores were simulated in 5, 10, or 30 replicates for increasing spot number and fitted using the SONIC approach. The SD of k_{min} values gradually decreased with the spot number. To see this figure in color, go online.

containing intensity fluctuations $\sigma = 0.10$ and mean intensity variations $\sigma_{mean} = 0.15$, we correctly predicted the fluorophore numbers $n = 1$, 4, and 10 with 1.0 ± 0.1, 4.1 ± 0.7, and 10.0 ± 1.6. Thus, fluctuations of mean intensities between traces in the range of the experimentally observed one did not bias the determination of the fluorophore number. Furthermore, this indicated that the homogeneity of trace intensities within each region was sufficient for an accurate analysis. This simulation may also indicate that the estimations provided by the approach would be accurate when molecules differ in their vertical position. In this case, wide-field and laser-scanning excitation could be an alternative to total internal reflection excitation as they would allow a more uniform illumination around the focal plane. In particular, the decrease of the signal to noise ratio with those approaches may be compensated by the robustness to noise of the SONIC analysis (Fig. 4 *B*).

To characterize the precision of the approach depending on both the fluorophore number and intensity fluctuations, we simulated spots with fluorophore numbers up to 30 as before and set the noise level of the signal to $\sigma = 0.0$, 0.2, 0.4, or 0.8. Notably, we observed that the relative standard deviation of the estimated fluorophore number remained constant for increasing fluorophore number and did not depend on the degree of noise (Fig. 4 *C*). In our SMPB measurements of tetra-DNA probes, we noticed that the standard deviation of the fitted fluorophore number decreased when the mean spot number per region increased from 10 to 30. To check the relevance of this observation, we applied our analysis on simulated spots with four fluorophores, for spot numbers per replicate from 1 to 30 and for different replicate numbers. Although robust, unbiased estimates could be obtained with spot numbers starting from ~7 (Fig. S9), increasing the spot number per region, but not the replicate number, improved the precision of the fluorophore number estimation, explaining the experimentally observed differences (Fig. 4 *D*).

Blinking is a typical biophysical behavior of fluorescent molecules. The dyes used in this study rarely showed strong blinking events. We would like to note that blinking occurring on a timescale that is much faster than the experimental frame duration would be averaged in the intensity traces and should therefore have no influence on the SONIC outcome. Nevertheless, to get further insights into the impact of blinking, we simulated scenarios with different blinking rates that generate clearly visible effects on the intensity traces (Fig. S10). From them, we observed that rare and short-lived off-states were tolerated by the SONIC approach (Fig. S10, *A*, *B*, and *E*) and that frequent blinking and long-lived off-states can lead to overestimation of the fluorophore number (Fig. S10, *C* and *D*). Thus, to estimate the fluorophore number/stoichiometry of molecule complexes using the SONIC approach, we recommend the use of dyes showing no pronounced blinking, or instead, the use of buffers in which blinking is attenuated.

One important aspect of our method is that it is based on the average behavior of several traces. As a consequence, on the other hand, when deviations from the theoretical

behavior are biased in one direction, such as blinking that shifts down the average intensity without affecting the spot number, they can bias the outcome of the SONIC approach. Likewise, we observed that blinking between two spectral forms of the dye can also lead to overestimation of the fluorophore number, as tested through simulations (Fig. S11, *A* and *B*). However, the intensity shifts experimentally seen with Atto647N should not have affected the estimation (Fig. S11 *C*). On the other hand, when deviations from the theoretical behavior are distributed symmetrically around the mean, such as with noise or fluctuations of initial intensities, they should not bias the results (Fig. 4 *B*).

Finally, in SMPB experiments, a low labeling efficiency, for example, because of photobleached molecules before the start of the experiment or because of nonmature fluorescent proteins, would lead to a systematic underestimation of the fluorophore number if not taken into account. To assess the extent of this underestimation, we simulated photobleaching of insufficiently labeled complexes for $n = 1$ to 30 fluorophores per spot, which was achieved by randomly assigning intensity values of fluorophores in the population to zero. First, we chose a labeling fraction of $\alpha = 0.7$, close to reported values (34). We then fitted the fluorophore number assuming $\alpha = 1$ using Eqs. 2 and 3. As anticipated, the fluorophore number was underestimated with the exception of $n = 1$, for which the estimation was correct (Fig. 5 *A*). Interestingly, we observed that the fluorophore number estimates corresponded well to the product of the expected fluorophore number with the labeling fraction ($k_{min,\alpha} = n * \alpha$, Fig. 5 *A*). Second, we confirmed this observation for different labeling fractions and for different fluorophore numbers (Fig. S12 *A*). We also observed that both parameters k and α cannot be fitted simultaneously (Fig. S12 *B*). Nonetheless, when we imposed the known value of the labeling fraction in the fit, as tested for six different labeling degrees ranging from $\alpha = 0.5$ to 1 and for fluorophore numbers of $n = 1$, 3, and 10, respectively, then we globally obtained the expected mean fluorophore number (Fig. 5 *B*). Thus, when assuming $\alpha = 1$, the approach delivers an estimate of the product of the real labeling fraction with the fluorophore number n that one would observe if α was 1. To summarize this part, the fluorophore number per spot can be estimated without bias if the labeling fraction is a priori known, for example when this fraction is experimentally controlled (35) or measured with a well-characterized calibration (13). Alternatively, one could also use the approach to estimate the labeling fraction from complexes of known stoichiometry.

From this last observation, we foresee potential applications of the approach in live cell imaging. From our experience, a typical limitation of SMPB in cells is the presence of autofluorescence that can strongly compete with the specific signal. In case this autofluorescence bleaches faster than the signal of interest, one could define a new time 0 for the analysis of the signal when autofluorescence becomes insignificant. Although one would miss the first bleaching events, one could extrapolate the fluorescence intensity decay to the time when illumination starts to estimate the fraction of fluorescence lost during the autofluorescence time window. This estimate could then be used in Eq. 4 to derive the fluorophore number. Testing this workflow on fixed cells will be a first step toward that aim. In living cells, one additionally needs to account for receptor movements. The strategy presented in this study used the intensity traces of individual spots and therefore, the analysis of moving complexes would involve spot tracking. Alternatively, because the SONIC approach only requires the number of spots over time and their total intensity, one could extract the intensity without identification of individual spots and therefore without tracking. The main requirement will be that the spots remain within the field of illumination during the experiment and experience on average the same photobleaching probability.

CONCLUSIONS

The developed SONIC method represents a novel approach, to our knowledge, to estimate fluorophore numbers from SMPB data. By relating the spot number decay to the intensity decay, we can accurately measure the average fluorophore number from DNA probes containing one or four Atto-dyes and determine the trimeric state of GFP-tagged

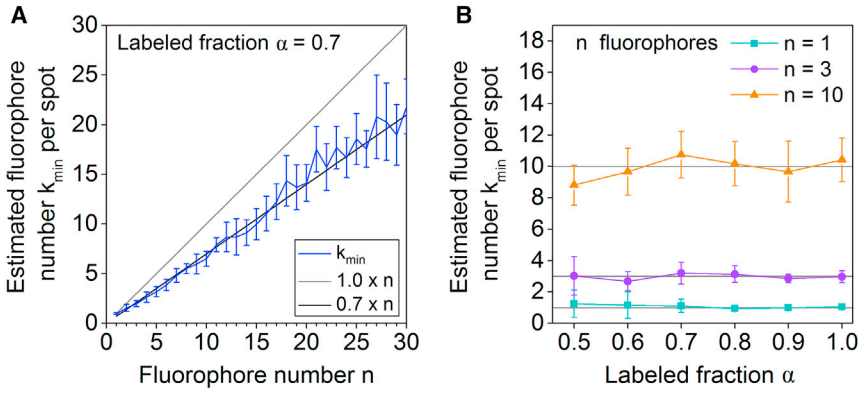

FIGURE 5 Influence of the labeling fraction on the determination of the fluorophore number. Simulations of 14 spots containing intensity fluctuations $\sigma = 0.4$. Mean and SD of 10 replicates. (*A*) Simulation for different fluorophore numbers n where 70% of fluorophores in the spot population are visible ($\alpha = 0.7$). The fit assuming $\alpha = 1$, using Eqs. 2 and 3 (*blue line*) led to an underestimation of the true fluorophore number (*gray line*) by a factor corresponding to the labeling fraction (*black line*), except for $n = 1$. (*B*) Simulation of spots with $n = 1$, 3, and 10 fluorophores. When the value of the labeling fraction is imposed in the fit using Eq. 4, the fluorophore number can be correctly estimated. To see this figure in color, go online.

sCD95L at picomolar concentration. Although the analysis generates an absolute estimate of the fluorophore number, it should be performed with the consideration of labeling efficiency that can be determined by use of calibration constructs. Taken together, the straightforward implementation of the SONIC approach, not requiring the detection of all photobleaching steps from SMPB data and its potential to estimate the fluorophore number even for high numbers makes it an attractive alternative to step detection approaches.

SUPPORTING MATERIAL

Supporting Materials and Methods and twelve figures are available at http://www.biophysj.org/biophysj/supplemental/S0006-3495(15)01111-X.

AUTHOR CONTRIBUTIONS

C.L. and J.B. conceived the method. C.L. designed, expressed, and characterized proteins. K.S.G. prepared DNA probes. K.S.G. and M.L. performed TIRF microscopy. S.W. and K.R. optimized intensity fitting of spots and provided the software. C.L. analyzed intensity-time profiles and performed computer simulations. D.H. and R.E. supervised the work. C.L. wrote the article with help by J.B. J.B. and R.E. should be considered as equal last authors. All authors contributed to the method design, discussion of the results, and writing of the manuscript. All authors have given approval to the final version of the manuscript.

ACKNOWLEDGMENTS

R.E., C.L., and J.B. and thank the Initiative and Networking Fund of the Helmholtz Association within the Helmholtz Alliance on Systems Biology/SBCancer. D.H., K.S.G., and M.L. thank the Deutsche Forschungsgemeinschaft and the CellNetworks Cluster of Excellence (DFG, EXC81, and GRK1114) for financial support. This work was partially funded via grants by the German Federal Ministry of Education and Research (BMBF) project e:BIO: ImmunoQuant (0316170A). The authors thank Dr. Christian Conrad for helpful advice.

SUPPORTING CITATIONS

References (36–40) appear in the Supporting Material.

REFERENCES

1. Chen, Y., J. Johnson, …, J. D. Mueller. 2010. Observing protein interactions and their stoichiometry in living cells by brightness analysis of fluorescence fluctuation experiments. *Methods Enzymol.* 472:345–363.
2. Herrick-Davis, K., E. Grinde, …, J. E. Mazurkiewicz. 2012. Oligomer size of the serotonin 5-hydroxytryptamine 2C (5-HT2C) receptor revealed by fluorescence correlation spectroscopy with photon counting histogram analysis: evidence for homodimers without monomers or tetramers. *J. Biol. Chem.* 287:23604–23614.
3. Sauer, M. 2013. Localization microscopy coming of age: from concepts to biological impact. *J. Cell Sci.* 126:3505–3513.
4. Grußmayer, K. S., A. Kurz, and D. P. Herten. 2014. Single-molecule studies on the label number distribution of fluorescent markers. *Chem. Phys. Chem.* 15:734–742.
5. Kurz, A., J. J. Schmied, …, D. P. Herten. 2013. Counting fluorescent dye molecules on DNA origami by means of photon statistics. *Small.* 9:4061–4068.
6. Zhang, H., and P. Guo. 2014. Single molecule photobleaching (SMPB) technology for counting of RNA, DNA, protein and other molecules in nanoparticles and biological complexes by TIRF instrumentation. *Methods.* 67:169–176.
7. Arant, R. J., and M. H. Ulbrich. 2014. Deciphering the subunit composition of multimeric proteins by counting photobleaching steps. *Chem. Phys. Chem.* 15:600–605.
8. Fricke, F., M. S. Dietz, and M. Heilemann. 2015. Single-molecule methods to study membrane receptor oligomerization. *Chem. Phys. Chem.* 16:713–721.
9. Coffman, V. C., and J. Q. Wu. 2012. Counting protein molecules using quantitative fluorescence microscopy. *Trends Biochem. Sci.* 37:499–506.
10. Shu, D., H. Zhang, …, P. Guo. 2007. Counting of six pRNAs of phi29 DNA-packaging motor with customized single-molecule dual-view system. *EMBO J.* 26:527–537.
11. Ulbrich, M. H., and E. Y. Isacoff. 2007. Subunit counting in membrane-bound proteins. *Nat. Methods.* 4:319–321.
12. Das, S. K., M. Darshi, …, H. Bayley. 2007. Membrane protein stoichiometry determined from the step-wise photobleaching of dye-labelled subunits. *Chem. Bio. Chem.* 8:994–999.
13. McGuire, H., M. R. Aurousseau, …, R. Blunck. 2012. Automating single subunit counting of membrane proteins in mammalian cells. *J. Biol. Chem.* 287:35912–35921.
14. Leake, M. C., J. H. Chandler, …, J. P. Armitage. 2006. Stoichiometry and turnover in single, functioning membrane protein complexes. *Nature.* 443:355–358.
15. Coffman, V. C., P. Wu, …, J. Q. Wu. 2011. CENP-A exceeds microtubule attachment sites in centromere clusters of both budding and fission yeast. *J. Cell Biol.* 195:563–572.
16. Zhang, H., D. Shu, …, P. Guo. 2007. Instrumentation and metrology for single RNA counting in biological complexes or nanoparticles by a single-molecule dual-view system. *RNA.* 13:1793–1802.
17. Simonson, P. D., H. A. Deberg, …, P. R. Selvin. 2010. Counting bungarotoxin binding sites of nicotinic acetylcholine receptors in mammalian cells with high signal/noise ratios. *Biophys. J.* 99:L81–L83.
18. Kerssemakers, J. W., E. L. Munteanu, …, M. Dogterom. 2006. Assembly dynamics of microtubules at molecular resolution. *Nature.* 442:709–712.
19. Vogelsang, J., R. Kasper, …, P. Tinnefeld. 2008. A reducing and oxidizing system minimizes photobleaching and blinking of fluorescent dyes. *Angew. Chem. Int.Engl.* 47:5465–5469.
20. Gust, A., A. Zander, …, D. Grohmann. 2014. A starting point for fluorescence-based single-molecule measurements in biomolecular research. *Molecules.* 19:15824–15865.
21. Snapp, E. L., R. S. Hegde, …, J. Lippincott-Schwartz. 2003. Formation of stacked ER cisternae by low affinity protein interactions. *J. Cell Biol.* 163:257–269.
22. Walczak, H., R. E. Miller, …, D. H. Lynch. 1999. Tumoricidal activity of tumor necrosis factor-related apoptosis-inducing ligand in vivo. *Nat. Med.* 5:157–163.
23. Schwering, M., A. Kiel, …, D. P. Herten. 2011. Far-field nanoscopy with reversible chemical reactions. *Angew. Chem. Int.Engl.* 50:2940–2945.
24. Wörz, S., P. Sander, …, K. Rohr. 2010. 3D geometry-based quantification of colocalizations in multichannel 3D microscopy images of human soft tissue tumors. *IEEE Trans. Med. Imaging.* 29:1474–1484.
25. Berg, D., M. Lehne, …, H. Wajant. 2007. Enforced covalent trimerization increases the activity of the TNF ligand family members TRAIL and CD95L. *Cell Death Differ.* 14:2021–2034.
26. Tanaka, M., T. Suda, …, S. Nagata. 1995. Expression of the functional soluble form of human fas ligand in activated lymphocytes. *EMBO J.* 14:1129–1135.

27. Corti, A., G. Fassina, …, G. Cassani. 1992. Oligomeric tumour necrosis factor alpha slowly converts into inactive forms at bioactive levels. *Biochem. J.* 284:905–910.

28. Poiesi, C., A. Albertini, …, A. Corti. 1993. Kinetic analysis of TNF-alpha oligomer-monomer transition by surface plasmon resonance and immunochemical methods. *Cytokine.* 5:539–545.

29. Harbury, P. B., P. S. Kim, and T. Alber. 1994. Crystal structure of an isoleucine-zipper trimer. *Nature.* 371:80–83.

30. Chattopadhyay, K., U. A. Ramagopal, …, S. C. Almo. 2007. Assembly and structural properties of glucocorticoid-induced TNF receptor ligand: Implications for function. *Proc. Natl. Acad. Sci. USA.* 104: 19452–19457.

31. Smith, R. A., and C. Baglioni. 1987. The active form of tumor necrosis factor is a trimer. *J. Biol. Chem.* 262:6951–6954.

32. Zhou, Z., X. Song, …, M. I. Greene. 2008. Human glucocorticoid-induced TNF receptor ligand regulates its signaling activity through multiple oligomerization states. *Proc. Natl. Acad. Sci. USA.* 105: 5465–5470.

33. Durisic, N., L. Laparra-Cuervo, …, M. Lakadamyali. 2014. Single-molecule evaluation of fluorescent protein photoactivation efficiency using an in vivo nanotemplate. *Nat. Methods.* 11:156–162.

34. Hines, K. E. 2013. Inferring subunit stoichiometry from single molecule photobleaching. *J. Gen. Physiol.* 141:737–746.

35. Cherny, D., C. Gooding, …, I. C. Eperon. 2010. Stoichiometry of a regulatory splicing complex revealed by single-molecule analyses. *EMBO J.* 29:2161–2172.

36. Humphrey, W., A. Dalke, and K. Schulten. 1996. VMD: visual molecular dynamics. *J. Mol. Graph.* 14:33–38.

37. Bloomfield, V. A. 2000. Survey of biomolecular hydrodynamics. *In* Separations and Hydrodynamics. On-Line Biophysics Textbook. Biophysics Society, Rockville, MD. *www.biophysics.org*.

38. Magde, D., E. L. Elson, and W. W. Webb. 1974. Fluorescence correlation spectroscopy. II. An experimental realization. *Biopolymers.* 13:29–61.

39. Rasband, W. S. 1997–2014. ImageJ. U. S. National Institutes of Health, Bethesda, MD. *http://imagej.nih.gov/ij/*.

40. Shaner, N. C., R. E. Campbell, …, R. Y. Tsien. 2004. Improved monomeric red, orange and yellow fluorescent proteins derived from *Discosoma sp.* red fluorescent protein. *Nat. Biotechnol.* 22:1567–1572.